

D2C-SR: A Divergence to Convergence Approach for Image Super-Resolution

Youwei Li¹ Haibin Huang² Lanpeng Jia¹ Haoqiang Fan¹ Shuaicheng Liu^{3,1}

¹Megvii Technology ²Kuaishou Technology

³University of Electronic Science and Technology of China

Abstract

In this paper, we present D2C-SR, a novel framework for the task of image super-resolution (SR). As an ill-posed problem, the key challenge for super-resolution related tasks is there can be multiple predictions for a given low-resolution input. Most classical methods and early deep learning based approaches ignored this fundamental fact and modeled this problem as a deterministic processing which often lead to unsatisfactory results. Inspired by recent works like SRFlow, we tackle this problem in a semi-probabilistic manner and propose a two-stage pipeline: a divergence stage is used to learn the distribution of underlying high-resolution outputs in a discrete form, and a convergence stage is followed to fuse the learned predictions into a final output. More specifically, we propose a tree-based structure deep network, where each branch is designed to learn a possible high-resolution prediction. At the divergence stage, each branch is trained separately to fit ground truth, and a triple loss is used to enforce the outputs from different branches divergent. Subsequently, we add a fuse module to combine the multiple predictions as the outputs from the first stage can be sub-optimal. The fuse module can be trained to converge w.r.t the final high-resolution image in an end-to-end manner. We conduct evaluations on several benchmarks, including a new proposed dataset with 8x upscaling factor. Our experiments demonstrate that D2C-SR can achieve state-of-the-art performance on PSNR and SSIM, with a significantly less computational cost.

1. Introduction

Super-resolution is one of the fundamental problems in computer vision with its applications for several important image processing tasks [25, 2]. Despite decades of development in image super-resolution technologies, it remains challenging to recover high quality and accurate details from low resolution inputs due to its ill-posed nature.

In fact, given a low-resolution image, there exist infinitely possible high-resolution predictions by adding dif-

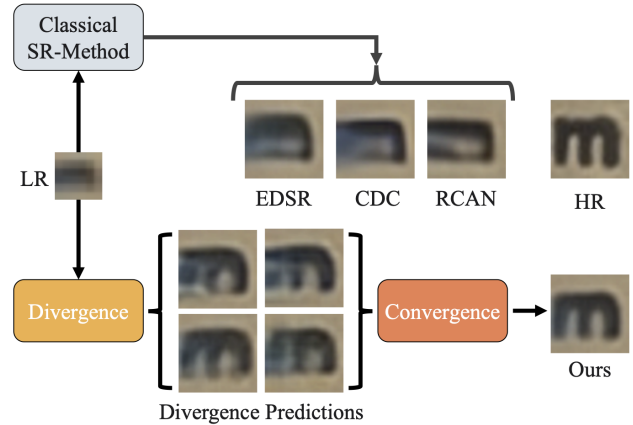


Figure 1. Classical super-resolution methods adopt direct end-to-end networks to solve the ill-posed problem. In contrast, our D2C network uses a tree structure to first generate divergent intermediate predictions in the divergence stage, and then we fuse these variants in the convergence stage for a more accurate prediction.

ferent high-frequency information. This is a key challenge for the design of learning-based super-resolution approaches. Recently, deep neural network (DNN) based methods [19, 13, 33] have achieved tremendous success and outperformed most classical methods based on sparse coding [9, 28] or local linear regression [23, 27]. However, these early deep learning methods only rely on L_1 or L_2 reconstruction loss, which can not reproduce sharp details in nature images. Later on, with the development of deep generative models, conditional GAN-based architecture [10] was adapted into SR tasks, which provide methods for learning the distribution in a data-driven way and led to more plausible SR results. However, these methods still suffered from mode collapse where they easily learn to ignore stochastic inputs and make the SR translation a purely deterministic mapping [12, 16, 4]. Recently, SRFlow [14] introduced a normalizing flow-based method which tried to address the mode collapse problem and make a step forward to modeling the real distribution of all possible SR reconstructions. While SRFlow did show promising SR-results by recover-

ing fine details, the Gaussian distribution it used limits the diversity of the possible outputs. Adapting more complicated distribution would significantly increase the hardness of convergence during training and inference.

In this paper, we introduce D2C-SR, a novel divergence to convergence framework for image super-resolution. D2C-SR follows the idea of learning the underlying distribution, but in a discrete setting. Unlike conditional GAN-based methods or SRFlow, D2C-SR does not explicitly model the distribution. Instead, we design the network for learning several most possible outputs. Our key insight is that, although there are infinitely possible HR images, the plausible ones are limited and located in ‘peaks’ of the real distribution. Towards this end, we first propose a tree-based structure deep network, where each branch is designed to learn a possible high resolution prediction. Since there is no ‘real peaks’ we can use as supervision, we train the network in a semi-supervised way: we use a triple loss to enforce the outputs from different branches are as divergence as possible together with a traditional L_2 loss to make sure each output is close to the ground truth HR image. Theoretically, if there are infinite branches, the best HR image should be one of the outputs. While in our discrete setting, the network generates several most possible outputs and the training could be sub-optimal. Hence, we further add a fuse module to combine the multiple predictions. The fuse module leans to interpolate over different output ‘peaks’ and generate a converged HR output.

To fully evaluate D2C-SR, we conduct experiments on several public benchmarks, including RealSR[7] and DRealSR[26], for real-world SISR. To fully explore the efficiency of D2C-SR, we further propose a new dataset, **D2CRealSR**, with 8x upscaling factor. Experimental results show that the proposed approach can outperform previous methods with significantly less computational cost and achieve state-of-the-art performance on PSNR and SSIM. To summarize, the main contributions are as follows:

- We present D2C-SR, a novel semi-probabilistic framework for image super-resolution. By decomposing SR into divergence and convergence stages, D2C-SR captures sufficient variations of underlying distributions, providing a convenient way for end-to-end inference.
- We propose to train the divergence in a semi-supervised manner, where a triplet loss is used to enforce the divergence of predictions.
- D2C-SR sets up new state-of-the-art performance on many popular benchmarks measured by PSNR and SSIM, including a new proposed dataset D2CRealSR with 8x upscaling factor. D2C-SR can also provide compatible performance with significantly less computational cost.
- We provide in-depth analysis to understand various design choices of the D2C-SR framework.

2. Related Work

2.1. DNN-based SISR

Single Image Super Resolution (SISR) is a long standing research topic due to its importance and ill-posed nature. Traditional learning-based methods adopts sparse coding [9, 20, 28] or local linear regression [23, 22, 27]. Deep learning (DL)-based methods have achieved dramatic advantages against conventional methods for SISR, which has been well documented in [25, 2]. It is first proposed by SRCNN [19] that employs a relatively shallow network and adopts the bicubic degradation for HR and LR pairs. Following which, various SISR approaches have been proposed, such as VDSR that adopts very deep network [19]; EDSR that modifies the ResNet for enhancement [13]; DnCNN that predicts high frequency details [30]; ESPCN that uses efficient sub-pixel CNN [18]; CDC that divides images into multiple regions [26], CARN that adopts cascading residual network [1]; and VGG loss [19], GAN loss [10] that improve the perceptual visual quality [12, 17, 24]. In this work, we propose a tree-based network structure, for the purpose of multi-mode learning.

2.2. Learning Super Resolution Space

Single image super-resolution is ill-posed, where infinitely many high-resolution images can be downsampled to the same low-resolution image. Therefore learning a deterministic mapping may not be optimal. The problem can be converted to stochastic mapping, where multiple plausible high-resolution images are predicted given a single low-resolution input [3]. DeepSEE incorporates semantic maps for explorative facial super-resolution [6]. SRFlow adopts normalizing flow to learn the conditional distribution of the output given the LR facial input [14]. In this work, unlike these approaches that formulate the problem as one-to-many stochastic mapping, we still learn a one-to-one deterministic mapping but allows many intermediate variants to increase the diversity of the network.

2.3. Datasets

The widely used datasets include Set5 [5], Set14 [29], BSD300 [15], Urban100 [11] and DIV2K [21]. As known, LR and HR pairs obtained from bicubic downsampling are inaccurate. Therefore, non-blind SR simulates the degradation process by sampling Gaussian filters and noise levels [31]. SR-RAW dataset captures the real-world scenes for image raw data through camera optical zoom [32]. RealSR dataset provides a well-prepared benchmark for real-world SISR [7]. DRealSR is a large-scale real-world SR benchmark that is collected from five DSLR cameras [26]. In this

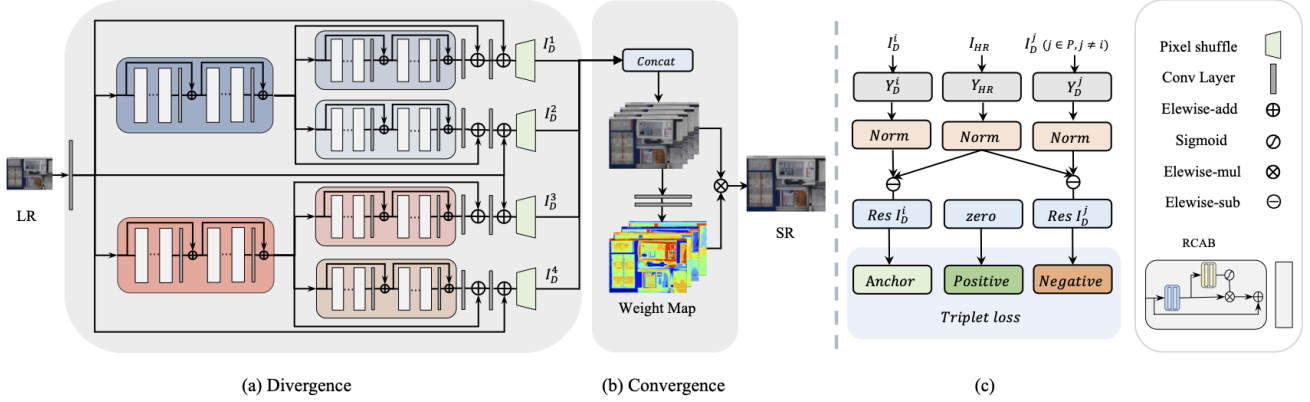


Figure 2. Our architecture consists of two stages, (a) Divergence stage and (b) Convergence stage. The divergence network with tree structure outputs multiple predictions I_D^i who has different high-frequency recovery. The goal of convergence network is to obtain more accurate result SR by weighted combining the results. (c) Triplet loss is used to train our network.

work, we mainly adopt RealSR and DRealSR for the evaluation. We also capture a dataset on our own with camera optical zoom for 8x evaluations.

3. Method

3.1. Overview

In this section, we formally introduce our proposed D2C-SR framework. As discussed in Section. 1, image super-resolution can be formulated as the problem of learning a conditional probability distribution of high-resolution images given a low-resolution input. However, it is in general hard to learn a full distribution for real nature images with complicate structure and textures. Therefore, we tackle this challenging problem in a discrete manner: we train a network to predict the limited number of possible high-resolution outputs with sufficient divergence to cover the full high-resolution image space. As shown in Figure. 3, compared with classical SR methods that generate one output, divergence outputs have a higher probability of being close to desired target, and we can approximate the target better by adding a fusing of the outputs. We name such divergence then convergence approach D2C-SR.

As shown in Figure. 2, D2C-SR consists of two sub-networks: a divergence network to learn the possible predictions and a convergence network to fuse the predictions to a final output. The rest of this section is organized as follow: we first describe divergence network in Section. 3.2. Then, we introduce convergence network in Section. 3.3. The network training details are described in Section. 3.4.

3.2. Divergence Network

In our divergence network, we address the ill-posed nature of SR by explicitly design a network to output multiple and divergent predictions. To be more specific, we

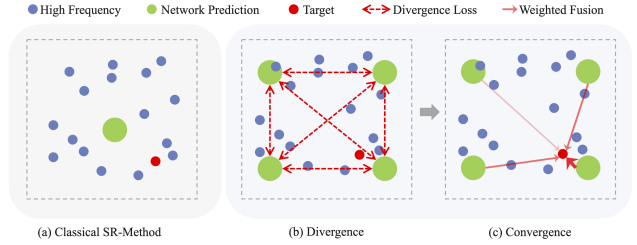


Figure 3. We show the difference between our method and the classical method in handling ill-posed problems. The classical method can only find a single prediction in the high-frequency domain. However, our method can differentiate into multiple predictions by divergence network and weighted fusion by convergence network to get a more accurate target.

built a tree-based structure network to get the desired predictions. There are three main modules in the divergence network: shallow feature extraction module, basic branch module, and upscale module. The network has L layers of branches, each of which is composed of a basic branch module and has C child branches. Basic branch module contains G residual groups. Each residual group further contains B residual channel attention blocks, similar as RCAN [33]. As shown in Figure. 2, the divergence network starts from a shallow feature extraction module, which consists of one convolutional layer and extracts the shallow feature from the input LR image. The shallow feature then go through the network layer by layer according to the tree structure. Note that the branches at each layer are not weight shared. The results of branches at final layer go through the deep residual structure and are upsampled by an upscale module. Finally, the divergence network generate P divergence predictions, which have different high frequency performances. These predictions are expressed

as $I_D = F(I_{LR}; \Theta_D)$, where Θ_D is the divergence network model parameter and I_{LR} is the LR image. I_D^i is denoted as i -th prediction of divergence network.

Deep Residual Structure We construct relatively deeper residuals in the divergence network. The intermediate features of branches at each layer in order to pass through a convolutional layer then added to owned leaf node features as shown in Figure. 2. The deep residual structure makes the branch of each layer learn a deep residual feature, and its child branches learn a deeper residual result based on themselves. Each of branches focuses on learning further residual based on the result of the father branch of previous layer, which facilitates high-frequency learning.

Divergence loss. Divergence loss used in divergence network, which composed of L_2 loss and triplet loss. Each of results I_D^i calculate L_2 loss separately with HR image and add up to form the final L_2 loss, which can be defined as

$$L_2^D = \sum_{i=1}^P \|I_D^i - I_{HR}\|_2. \quad (1)$$

In order to make the divergence network produce divergence results, we use triplet loss between all pairs of different predictions from divergence network. Our goal is to make the distance between I_D^i and HR close and make the distance farther between every two of the I_D set. However, using triplet loss directly on RGB images causes the network to focus more on other differentiated directions (e.g., RGB space and luminance) than texture features. Therefore, we first processed I_D^i using $G(\cdot)$:

$$G(I_D^i) = \frac{Y_D^i - \mu_{Y_D^i}}{\sigma_{Y_D^i}}, \quad (2)$$

where Y_D^i is Y channel of I_D^i , $\mu_{Y_D^i}$ and $\sigma_{Y_D^i}$ are mean and standard deviation of Y_D^i respectively. Add $G(\cdot)$ operation can make the network enable to focus more on the differentiation of texture features between I_D^i . Because the ill-posed problem is mainly raised in the high frequency area, our triplet loss is calculated on the residual domain. We express the residual of I_D^i as

$$res_{I_D^i} = |G(I_D^i) - G(I_{HR})|, \quad (3)$$

where $|\cdot|$ is absolute value function. It can reduce the checkerboard phenomenon caused by triplet loss. The formula for triplet loss is

$$trip(a, p, n) = \text{Max}[d(a, p) - d(a, n) + \text{margin}, 0], \quad (4)$$

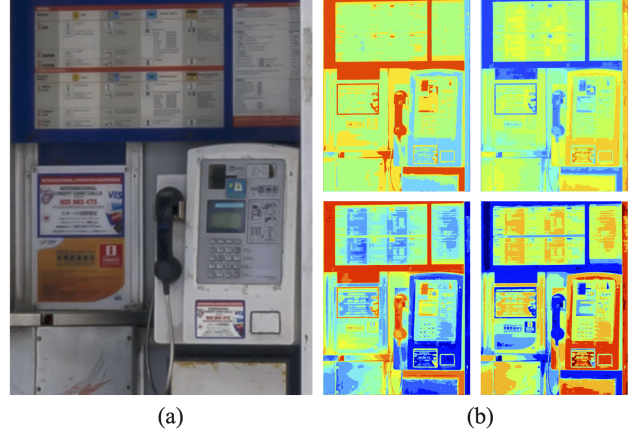


Figure 4. Weight map in our convergence stage. (a) the example. (b) are weights learned to combine for the final result. The weights are normalized to $0 \sim 1$. Red indicates higher values, while the blue indicates lower values. The top and the bottom belong to a large tree branch, within which left and right belongs to sub-branches (Our basemodel $L = 2$, $C = 2$).

where a , p and n are anchor, positive and negative, respectively. Therefore, we can represent our final triplet loss as

$$T_D = \frac{\sum_{i=1}^P \sum_{j=1, j \neq i}^P \beta_{ij} * trip(res_{I_D^i}, zero, res_{I_D^j})}{(P(P-1))}, \quad (5)$$

where $zero$ is zero map because we calculate triplet loss on residual domain. And β is a attenuation coefficient which can be described as

$$\beta_{ij} = \theta^{l-1}, l \in [1, L], \quad (6)$$

where θ is parameter and $\theta \in (0, 1]$. The l is the number of layers where the common parent node of I_D^i and I_D^j is located. We use β because that two branches belonging to the same parent node in deeper layer have a lower degree of discrimination relatively. Finally, our divergence loss is described as

$$L_D = L_2^D + \alpha * T_D, \quad (7)$$

where α is weight hyperparameter of T_D . Some detailed parameter settings will be introduced in Sec. 4.1

3.3. Convergence Network

Combining the divergence results generated by the divergence network can produce more accurate results. We think that different areas on the predictions have different contribution weights for the final result. So we construct convergence network to merge divergent results weighted pixel-by-pixel, which can generate the result closer to the real HR image. Convergence network concatenates all the M predictions of the divergence network and outputs a weight

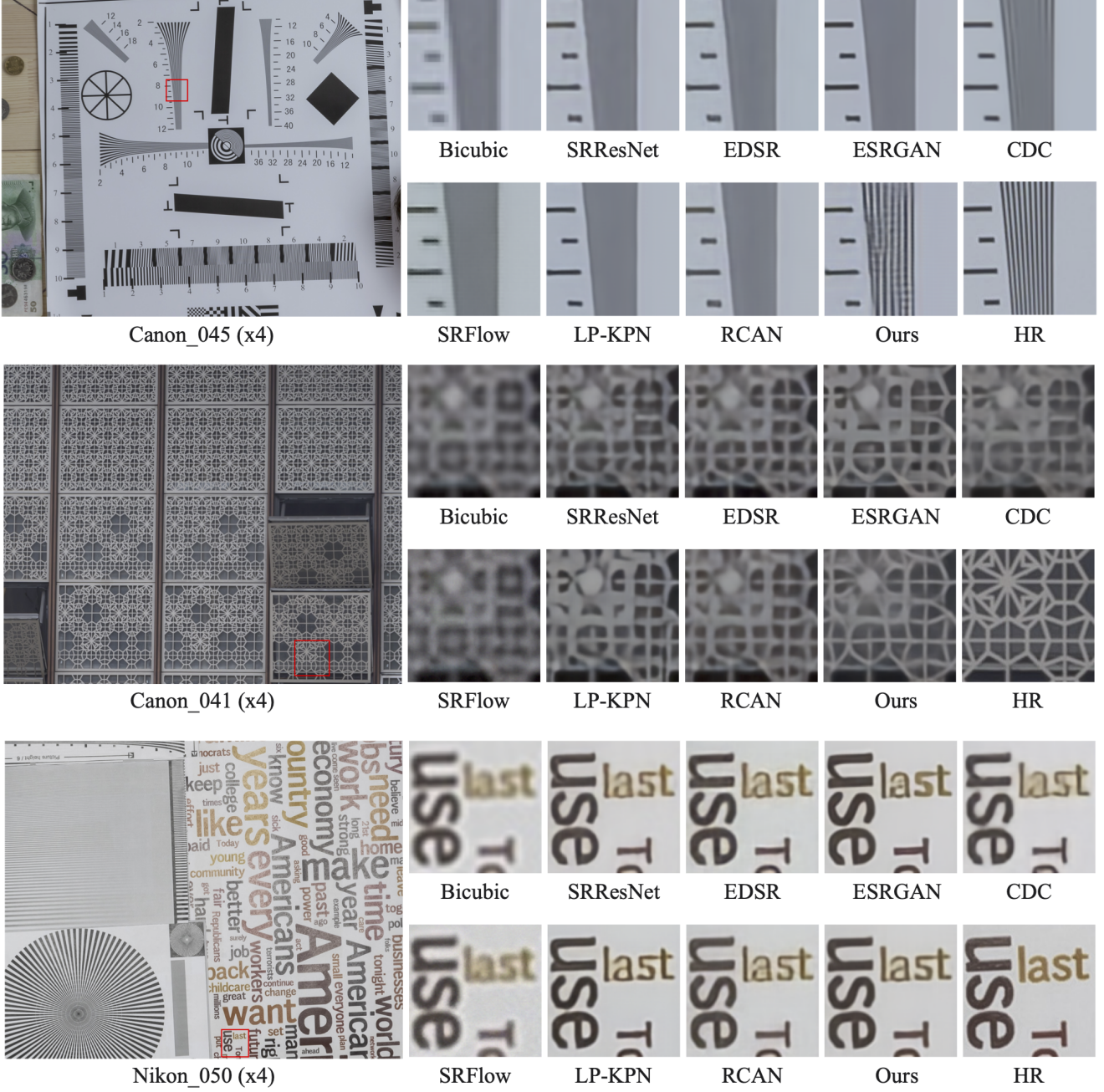


Figure 5. SR results for x4 on RealSR [7] and x8 on D2CRealSR in comparison with state-of-the-art approaches. We choose to compare with Bicubic, SRResNet [12], EDSR [13], ESRGAN [24], CDC [26], SRFlow [14], LP-KPN [7], and RCAN [33]. Our results are consistently better than the compared methods. In particular, for the case Canon-045, only our method can recover the ‘stripe’ texture.

map for each prediction I_D^i . Weight maps can be expressed as $W = F(\text{Concat}(I_D); \Theta_C)$, where Θ_C is the convergence network model parameter and Concat is the concat function. We denote W_i as the weight map of I_D^i . Every I_D^i are element-wise multiplied by respective weight map W_i , and then all of the results are summed to produce the final

SR result. Accordingly, SR result can be defined as

$$I_{SR} = \sum_{i=1}^P (I_D^i \cdot W_i), \quad (8)$$

where I_{SR} represents final SR result. P is the number of results produced by the divergence network. In Figure. 4,

We show an example of a weight map using the way of the heatmap. We can see that every prediction has different weights in different areas during the merge process.

Convergence loss. The goal of convergence network is to merge I_D^i from divergence network. Therefore loss function of convergence network is called convergence loss, which only consists of L_2 loss. We denote convergence loss as L_2^C , which can be expressed as

$$L_2^C = \|I_{SR} - I_{HR}\|_2. \quad (9)$$

How to generate I_{SR} has been introduced in Eq. 8. The optimization goal of convergence loss is to make the generated SR image get close to the ground-truth HR image.

3.4. Training Strategy

The two networks in our framework are trained separately. We firstly train the divergence network into a stable status where it can generate super-resolution divergence predictions. We then freeze the parameters of divergence network and train the convergence network by enabling the whole pipeline. More details will be discussed in Sec. 4.1.

4. Experiment

4.1. Dataset and Implementation Details

D2CRealSR. The existing RealSR datasets generally include x2, x3 and x4 scale factor only but lack of data for the larger scale factor. We collect a new dataset on x8 scale factor, which called D2CRealSR. We construct the LR and HR pairs by zooming the lens of DSLR cameras. D2CRealSR consists of 115 image pairs and 15 image pairs are selected randomly for testing set; the rest pairs construct the training set. We use SIFT method to register the image pairs iterative: we first register the image pairs roughly and crop the main central area, then we align the brightness of the central area of image pairs and register them once again. After that, we crop off the edges of aligned image pairs. The image size of each pair is $3,456 \times 2,304$ after the alignment process. We will release our D2CRealSR dataset later.

Existing Datasets. We also conduct experiments on existing real-world SR datasets: RealSR and DRealSR. RealSR has 559 scenes captured from Nikon and Canon DSLR cameras and align the image pairs strictly. 459 scenes are selected for training and 100 scenes for testing. The image sizes of RealSR image pairs are in the range of 700~3000 and 600~3500. DRealSR has 83, 84 and 93 image pairs in testing set, 884, 783 and 840 image pairs in training set for x2, x3, x4 scale factors, respectively. Note that we found some of the image pairs in DRealSR are misaligned, which

is caused by the depth of field. So we only validate our results on testing set of DRealSR to show the performance of the cross-dataset of our method.

Implementation Details. In the experiment, we set the number of branch layers as $L = 2$, the number of child branches $C = 2$. The basic branch module include $G = 2$ residual groups and $B = 4$ residual blocks in each group. We use Adam optimizer and set exponential decay rates as 0.9 and 0.999. The initial learning rate is set to 10^{-4} and then reduced to half every $2k$ epochs. For each training batch, we randomly extract 4 LR image patches with the size of 96×96 . We implement D2C method with the Pytorch framework and train the network using NVIDIA 2080Ti GPU.

4.2. Comparisons with Existing Methods

To evaluate our method, we train and test our model on our D2CRealSR with scale factor x8 and an existing real-world SR dataset, RealSR with scale factor x4, x3, x2. In addition, we validate on DRealSR testing set for performance of cross-dataset. We compare our model with other state-of-the-art SISR methods, including SRResNet [12], EDSR [13], RCAN [33], ESRGAN [24], LP-KPN [7] and CDC [26]. The SISR results were evaluated on the Y channel in the YCbCr space using PSNR and SSIM. Among these SR methods, EDSR [13] and RCAN [33] are the classic SISR methods. In addition, LP-KPN [7] and CDC [26] are designed to solve the real-world SR problem. Especially, CDC outperforms the state-of-the-art algorithms on real-world SR dataset.

Quantitative comparison. The evaluation result of the SR method, including our model and the other 7 methods are demonstrated in Table 1. Red numbers denote the highest scores, while blue numbers denote the second-highest scores. Our model outperforms by a large margin on different up-scaling factors and test datasets.

Qualitative comparison. Some result of state-of-the-art SR methods and ours are shown in Figure. 5 and Figure. 6. It is observed that existing SR methods (e.g., RCAN, LP-KPN, CDC) tend to restore the details to be thicker, blurry, or unnatural. Meanwhile, we restore more high-frequency details than other methods in the first example. Further, our proposed D2C restore images with more natural details compared to other methods in other cases.

4.3. Model Size Analyses

We show comparisons about model size and performance in Figure. 8. We list six sizes of models: 5.88M, 4.53M, 3.63M, 0.91M, 0.23M and 0.19M. These models are

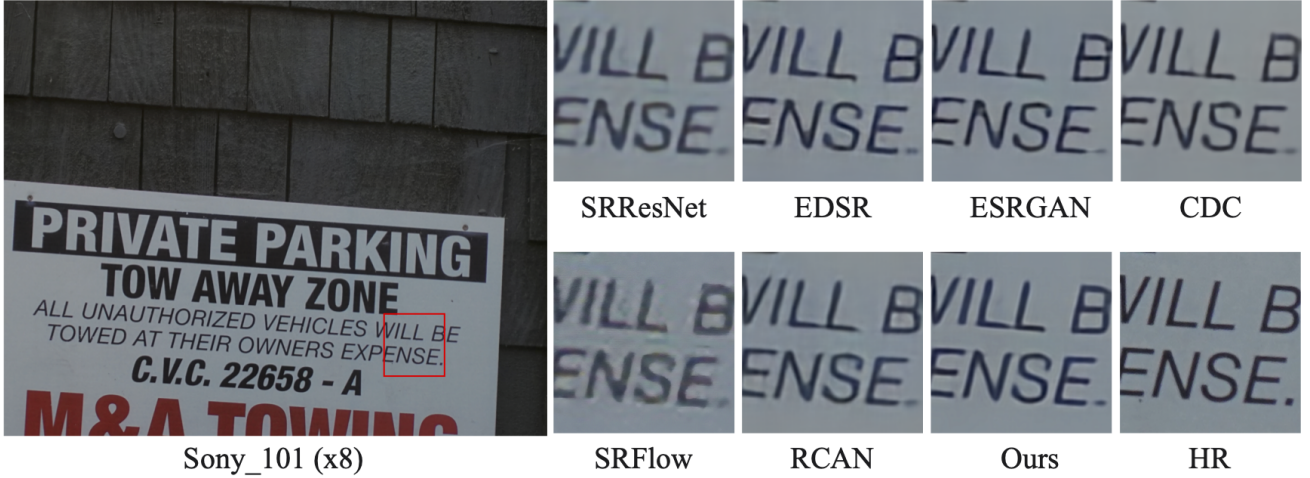


Figure 6. SR results for x8 on our captured D2CRealSR in comparison with state-of-the-art approaches. We choose to compare with SRResNet [12], EDSR [13], ESRGAN [24], CDC [26], SRFlow [14] and RCAN [33]. Our method can produce sharper edges.

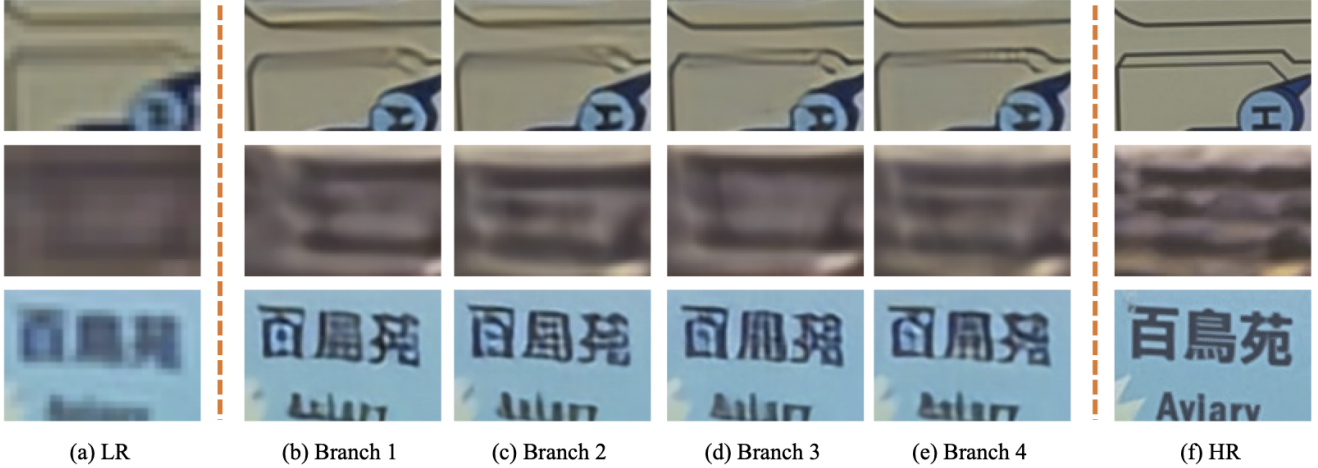


Figure 7. Demonstration of the intermediate divergent predictions. Row 1: (b) and (c) try to merge the two lines while (d) and (e) want to separate them. Row 2: In the middle region, (b), (c) and (e) restore the middle step, while (d) does not. Row 3: For the text region, the four branches have their own flavor. Each character is different from the others.

constructed by changing the number of residual groups G and the number of residual block B . Our 0.23M model can achieve a better effect than other methods. At this PSNR level, CDC uses 39.92M, and RCAN also uses 15M parameters. Our baseline model use 5.88M achieve higher performance, having a better trade-off between model size and performance.

4.4. Ablation Studies

The Width and Depth of Tree: Our divergence network is a tree-based architecture. We set different L and C to provide experimental evaluations on the width and depth of the tree. Because increasing the depth and width increases

memory usage. So we do these experiments on a small baseline model, which has $G = 2$ residual groups and each group has $B = 1$ block. As show in Table 3, we increase the width and depth from 1 to 4 respectively. By increasing the width and depth of the tree, the performance of PSNR has a significant boost.

Triplet Loss: As mentioned in Sec. 3.2, the triplet loss is used to enforce the outputs from different branches divergent. We further exam the effectiveness of our triplet loss by removing the term of Eq. 5. As show in Table 2 "w/o. triplet loss", PSNR scores in different scores are all decreased, especially in 2x scale factor, the PSNR decreased

Method	RealSR						DRealSR (train on RealSR)						D2CRealSR	
	2x		3x		4x		2x		3x		4x		8x	
	PSNR	SSIM	PSNR	SSIM	PSNR	SSIM	PSNR	SSIM	PSNR	SSIM	PSNR	SSIM	PSNR	SSIM
Bicubic	31.67	0.887	28.61	0.810	27.24	0.764	32.67	0.877	31.50	0.835	30.56	0.820	27.74	0.822
SRResNet [12]	33.17	0.918	30.65	0.862	28.99	0.825	32.85	0.890	31.25	0.841	29.98	0.822	30.01	0.864
EDSR [13]	33.88	0.920	30.86	0.867	29.09	0.827	32.86	0.891	31.20	0.843	30.21	0.817	30.23	0.868
RCAN [33]	33.83	0.923	30.90	0.864	29.21	0.824	32.93	0.889	31.76	0.847	30.37	0.825	30.26	0.868
ESRGAN [24]	33.80	0.922	30.72	0.866	29.15	0.826	32.70	0.889	31.25	0.842	30.18	0.821	30.06	0.865
SR-Flow [14]	-	-	-	-	24.20	0.71	-	-	-	-	24.97	0.73	23.11	0.600
LP-KPN [7]	33.49	0.917	30.60	0.865	29.05	0.834	32.77	-	31.79	-	30.75	-	-	-
CDC [26]	33.96	0.925	30.99	0.869	29.24	0.827	32.80	0.888	31.65	0.847	30.41	0.827	30.02	0.841
Ours	34.40	0.926	31.334	0.871	29.72	0.831	33.42	0.892	31.80	0.847	30.80	0.825	30.55	0.871

Table 1. Performance comparison on RealSR [7], DRealSR [26] and our proposed D2CRealSR datasets. The best one marks in red and the second best are in blue. ‘-’ indicates either the available model is not supported for such a test, or the method is not open-sourced.

Method	2x		3x		4x	
	PSNR	SSIM	PSNR	SSIM	PSNR	SSIM
I_D^1 w/o. convergence	34.24	0.924	31.20	0.868	29.55	0.827
I_D^2 w/o. convergence	34.28	0.925	31.17	0.868	29.56	0.828
I_D^3 w/o. convergence	34.27	0.925	31.21	0.868	29.54	0.827
I_D^4 w/o. convergence	34.26	0.925	31.16	0.867	29.57	0.827
w/o. triplet loss	34.23	0.925	31.28	0.869	29.66	0.829
w/o. deep res	34.28	0.925	31.28	0.870	29.68	0.830
D2C(ours)	34.40	0.926	31.34	0.871	29.72	0.831

Table 2. Effect of each component in the proposed D2C. We compare the performance w/o convergence network, triplet loss as well as deep residual structure.

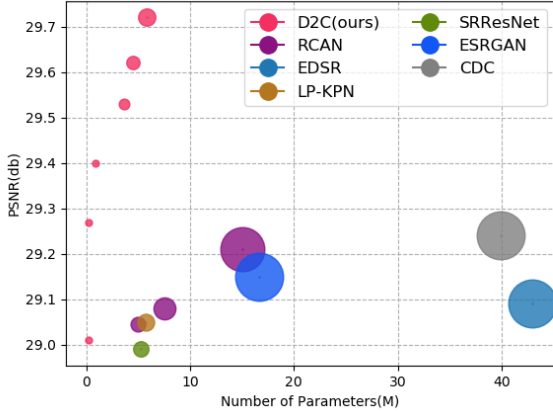


Figure 8. Performance vs. parameters on RealSR dataset.

	1	2	3	4
Width (C)	29.41	29.54	29.56	29.54
Depth (L)	29.30	29.54	29.63	29.64

Table 3. Effect study on the width and depth of the tree structure based network.

0.17 dB. Figure 7 shows the divergence effect of the image. As mentioned in the previous section, due to the existence

of triplet loss, the predictions of different branches show different high-frequency predictions. For the convenience of observation, we upscale the LR image with 4x scale factor. From (b) to (e) are the predictions of the four branches.

Convergence Network: To make sure that the improvement of convergence network, we remove the convergence network and save the result of each branch to compare with the convergence result showing in Table 2 “w/o. convergence”. It shows that the PSNR of the prediction of each branch is lower than the convergence result.

Deep Residual Structure: As mentioned in Sec. 3.4, the deep residual structure help network to focus on high-frequency information learning. We also disable the structure to verify its effectiveness. As show in Table 2 “w/o. deep res”. It shows that the PSNR decreased without the deep residual structure.

5. Conclusion

In this study, we revisit the problem of image super-resolution and provide a new two-stage approach: divergence stage for multiple predictions learning as well as convergence for predictions fusion. Instead of modeling the entire distribution, we propose to learn a limited number of

representative predictions and keep a sufficient divergence. This allows the network to be more efficient and achieves state-of-the-art performance with much less computational cost. We believe such divergence to convergence framework is a promising direction for image processing tasks like image inpainting as well as image denoising, and it is worth further exploration.

References

- [1] Namhyuk Ahn, Byungkun Kang, and Kyung-Ah Sohn. Fast, accurate, and lightweight super-resolution with cascading residual network. In *Proc. ECCV*, pages 252–268, 2018. [1](#), [2](#)
- [2] Saeed Anwar, Salman Khan, and Nick Barnes. A deep journey into super-resolution: A survey. *ACM Computing Surveys (CSUR)*, 53(3):1–34, 2020. [1](#), [2](#)
- [3] Yuval Bahat and Tomer Michaeli. Explorable super resolution. In *Proc. CVPR*, pages 2716–2725, 2020. [2](#)
- [4] Sefi Bell-Kligler, Assaf Shocher, and Michal Irani. Blind super-resolution kernel estimation using an internal-gan. In *Proc. NeurIPS*, 2019. [1](#)
- [5] Marco Bevilacqua, Aline Roumy, Christine Guillemot, and Marie Line Alberi-Morel. Low-complexity single-image super-resolution based on nonnegative neighbor embedding. In *Proc. BMVC*, 2012. [2](#)
- [6] Marcel C Buhler, Andrés Romero, and Radu Timofte. Deepsee: deep disentangled semantic explorative extreme super-resolution. In *Proc. ACCV*, 2020. [2](#)
- [7] Jianrui Cai, Hui Zeng, Hongwei Yong, Zisheng Cao, and Lei Zhang. Toward real-world single image super-resolution: A new benchmark and a new model. In *Proc. CVPR*, pages 3086–3095, 2019. [2](#), [5](#), [6](#), [8](#), [11](#)
- [8] Chang Chen, Zhiwei Xiong, Xinmei Tian, Zheng-Jun Zha, and Feng Wu. Camera lens super-resolution. In *Proc. CVPR*, pages 1652–1660, 2019. [11](#)
- [9] Dengxin Dai, Radu Timofte, and Luc Van Gool. Jointly optimized regressors for image super-resolution. In *Computer Graphics Forum*, volume 34, pages 95–104, 2015. [1](#), [2](#)
- [10] Ian J Goodfellow, Jean Pouget-Abadie, Mehdi Mirza, Bing Xu, David Warde-Farley, Sherjil Ozair, Aaron Courville, and Yoshua Bengio. Generative adversarial networks. *arXiv preprint arXiv:1406.2661*, 2014. [1](#), [2](#)
- [11] Jia-Bin Huang, Abhishek Singh, and Narendra Ahuja. Single image super-resolution from transformed self-exemplars. In *Proc. CVPR*, pages 5197–5206, 2015. [2](#)
- [12] Christian Ledig, Lucas Theis, Ferenc Huszár, Jose Caballero, Andrew Cunningham, Alejandro Acosta, Andrew Aitken, Alykhan Tejani, Johannes Totz, Zehan Wang, et al. Photo-realistic single image super-resolution using a generative adversarial network. In *Proc. CVPR*, pages 4681–4690, 2017. [1](#), [2](#), [5](#), [6](#), [7](#), [8](#), [11](#)
- [13] Bee Lim, Sanghyun Son, Heewon Kim, Seungjun Nah, and Kyoung Mu Lee. Enhanced deep residual networks for single image super-resolution. In *Proc. CVPRW*, pages 136–144, 2017. [1](#), [2](#), [5](#), [6](#), [7](#), [8](#), [11](#)
- [14] Andreas Lugmayr, Martin Danelljan, Luc Van Gool, and Radu Timofte. Srfnet: Learning the super-resolution space with normalizing flow. In *Proc. ECCV*, pages 715–732, 2020. [1](#), [2](#), [5](#), [7](#), [8](#)
- [15] David Martin, Charless Fowlkes, Doron Tal, and Jitendra Malik. A database of human segmented natural images and its application to evaluating segmentation algorithms and measuring ecological statistics. In *Proc. ICCV*, volume 2, pages 416–423, 2001. [2](#)
- [16] Haoyu Ren, Amin Kheradmand, Mostafa El-Khamy, Shuangquan Wang, Dongwoon Bai, and Jungwon Lee. Real-world super-resolution using generative adversarial networks. In *Proc. CVPRW*, pages 436–437, 2020. [1](#)
- [17] Mehdi SM Sajjadi, Bernhard Scholkopf, and Michael Hirsch. Enhancenet: Single image super-resolution through automated texture synthesis. In *Proc. ICCV*, pages 4491–4500, 2017. [2](#)
- [18] Wenzhe Shi, Jose Caballero, Ferenc Huszár, Johannes Totz, Andrew P Aitken, Rob Bishop, Daniel Rueckert, and Zehan Wang. Real-time single image and video super-resolution using an efficient sub-pixel convolutional neural network. In *Proc. CVPR*, pages 1874–1883, 2016. [2](#)
- [19] Karen Simonyan and Andrew Zisserman. Very deep convolutional networks for large-scale image recognition. *arXiv preprint arXiv:1409.1556*, 2014. [1](#), [2](#)
- [20] Libin Sun and James Hays. Super-resolution from internet-scale scene matching. pages 1–12, 2012. [2](#)
- [21] Radu Timofte, Eirikur Agustsson, Luc Van Gool, Ming-Hsuan Yang, and Lei Zhang. Ntire 2017 challenge on single image super-resolution: Methods and results. In *Proc. CVPRW*, pages 114–125, 2017. [2](#)
- [22] Radu Timofte, Vincent De Smet, and Luc Van Gool. Anchored neighborhood regression for fast example-based super-resolution. In *Proc. ICCV*, pages 1920–1927, 2013. [2](#)
- [23] Radu Timofte, Vincent De Smet, and Luc Van Gool. A+: Adjusted anchored neighborhood regression for fast super-resolution. In *Proc. ACCV*, pages 111–126, 2014. [1](#), [2](#)

- [24] Xintao Wang, Ke Yu, Shixiang Wu, Jinjin Gu, Yihao Liu, Chao Dong, Yu Qiao, and Chen Change Loy. Esrgan: Enhanced super-resolution generative adversarial networks. In *Proc. ECCVW*, pages 0–0. 2, 5, 6, 7, 8
- [25] Zhihao Wang, Jian Chen, and Steven CH Hoi. Deep learning for image super-resolution: A survey. 2020. 1, 2
- [26] Pengxu Wei, Ziwei Xie, Hannan Lu, Zongyuan Zhan, Qixiang Ye, Wangmeng Zuo, and Liang Lin. Component divide-and-conquer for real-world image super-resolution. In *Proc. ECCV*, pages 101–117, 2020. 2, 5, 6, 7, 8, 11
- [27] Chih-Yuan Yang and Ming-Hsuan Yang. Fast direct super-resolution by simple functions. In *Proc. ICCV*, pages 561–568, 2013. 1, 2
- [28] Jianchao Yang, John Wright, Thomas Huang, and Yi Ma. Image super-resolution as sparse representation of raw image patches. In *Proc. CVPR*, pages 1–8, 2008. 1, 2
- [29] Roman Zeyde, Michael Elad, and Matan Protter. On single image scale-up using sparse-representations. In *International conference on curves and surfaces*, pages 711–730, 2010. 2
- [30] Kai Zhang, Wangmeng Zuo, Yunjin Chen, Deyu Meng, and Lei Zhang. Beyond a gaussian denoiser: Residual learning of deep cnn for image denoising. *IEEE Trans. on Image Processing*, 26(7):3142–3155, 2017. 2
- [31] Kai Zhang, Wangmeng Zuo, and Lei Zhang. Learning a single convolutional super-resolution network for multiple degradations. In *Proc. CVPR*, pages 3262–3271, 2018. 2
- [32] Xuaner Zhang, Qifeng Chen, Ren Ng, and Vladlen Koltun. Zoom to learn, learn to zoom. In *Proc. CVPR*, pages 3762–3770, 2019. 2, 11
- [33] Yulun Zhang, Kunpeng Li, Kai Li, Lichen Wang, Biong Zhong, and Yun Fu. Image super-resolution using very deep residual channel attention networks. In *Proc. ECCV*, pages 286–301, 2018. 1, 3, 5, 6, 7, 8, 11

A. Supplementary Material

In this supplementary material, we first introduce more details of our D2CRealSR dataset in Sec. B, including the collection method and the processing method. Then, we show more visual results on D2CRealSR in Sec. C, and additional comparison results with other methods in Sec. D. Further, we provide more divergence results of the proposed D2C-SR method in Sec. E.

B. D2CRealSR Dataset

Existing real-world SISR datasets generally include images pairs on x2, x3 and x4 scale factors, such as RealSR dataset [7] and DRealSR dataset [26]. Our proposed D2CRealSR dataset have images pairs on x8 scale factor, which larger than the existing real-world datasets. The ill-posed problem is more obvious on D2CRealSR dataset.

Images pairs in our dataset are taken by zooming Sony α -7. The number of training pairs in our dataset is 100, and testing set has 15 images pairs selected randomly. The D2CRealSR provides, to the best of our knowledge, the first general purpose benchmark on x8 scale factor for real-world SISR. It is difficult to obtain images pairs with good alignment effects in natural scenes. These difficulties in the alignment process include depth-of-field misalignment, noticeable perspective misalignment, lens distortion misalignment and resolution alignment ambiguity [32]. Therefore, using the DSLR camera to directly acquire natural scene images pairs generally cannot be well aligned. We have found misalignment in DRealSR dataset, mostly due to depth-of-field misalignment. To solve these misalignment problems, we collect some high-resolution images, firstly. These images are mostly taken by DSLR from existing datasets or our own shooting dataset. Different from City100 [8], which only have city scenes, we have selected the images with different scenes including indoor and outdoor. It contains a variety of target objects with rich texture. Then, we make these pictures into postcards, and we get images pairs by taking photos of postcards. The postcard is on a fixed plane, which can reduce the influence of depth-of-field misalignment. It also weakens noticeable perspective misalignment. Further, we blur the HR images of pairs in during calculating matrix M in SIFT algorithm and apply the M on the source HR images to align source HR images with LR images. In this way, it can weaken the influence of resolution alignment ambiguity. We use multiple iterative alignment methods to ensure alignment results. Crop the center area after each alignment can reduce misalignment caused by lens distortion. Several examples of our D2CRealSR dataset are shown in Figure. 9, and it will be made publicly available later.

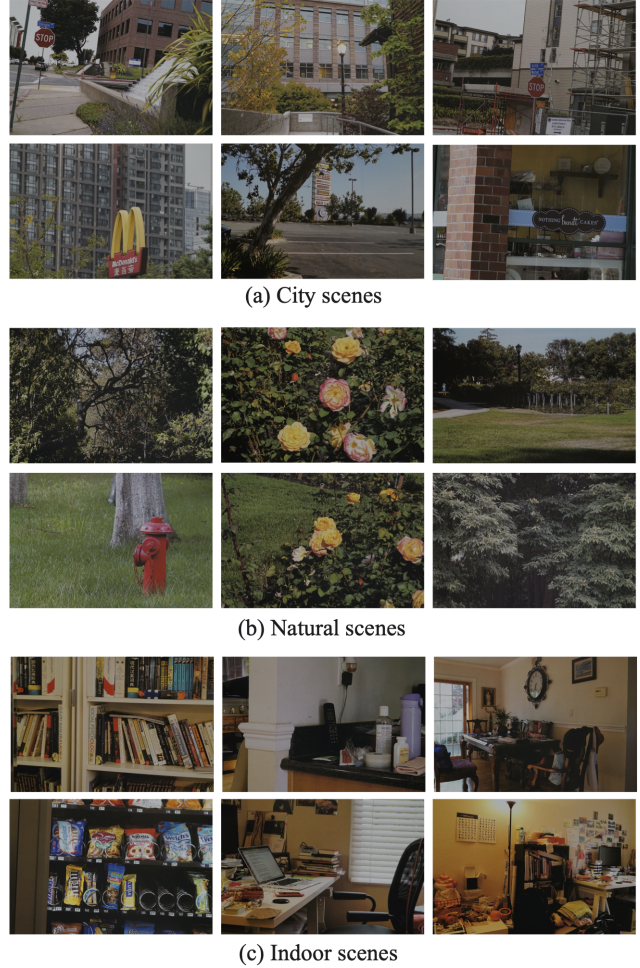


Figure 9. Examples of D2CRealSR dataset.

C. More Visual Results on D2CRealSR

In Figure. 10, we show more visual results from our proposed D2C-SR method on D2CRealSR dataset. We crop the images pairs and show the patch to facilitate the presentation of image details. The LR images patches are upsampled using bicubic method.

D. More Visual Comparison Results

We show more visual comparison results in Figure. 11. Our method is compared with other methods, SRResNet [12], EDSR [13], RCAN [33], CDC [26] and LP-KPN [7]. As shown in the figure, our proposed D2C-SR framework can restore more reasonable prediction results. Other classic super-resolution methods produce unnatural results due to the ill-posed problem.

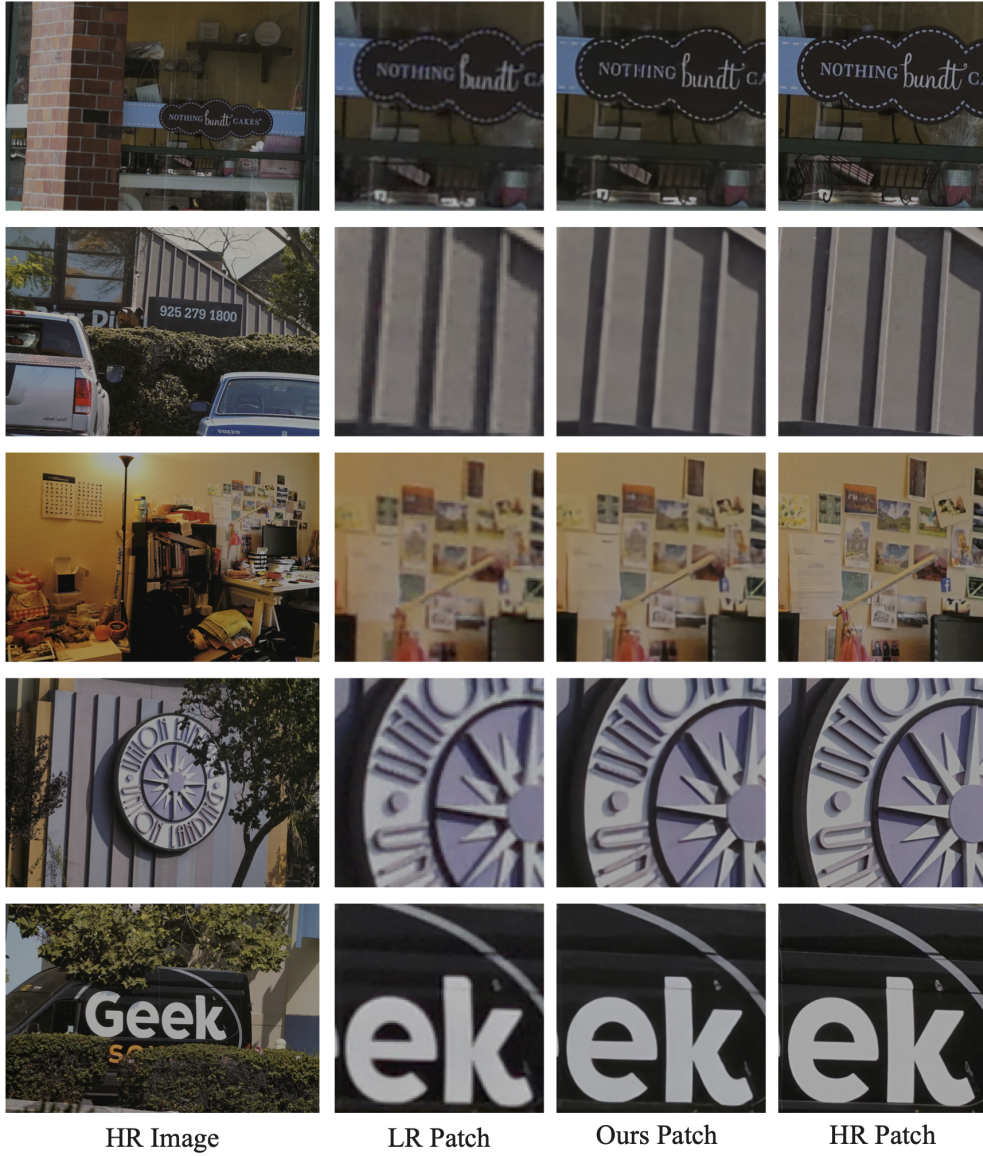


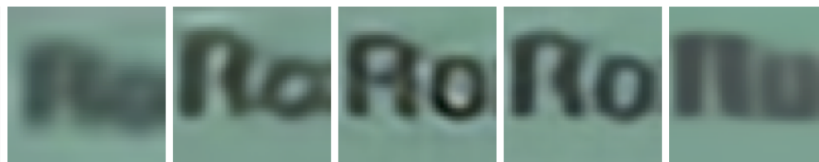
Figure 10. More visual results on D2CRealSR.

E. More Visual Divergence Results

We show more visual divergence results in Figure. 12. We also crop the images pairs, and the LR images patches are upsampled using bicubic method.



Nikon_010 (x4)



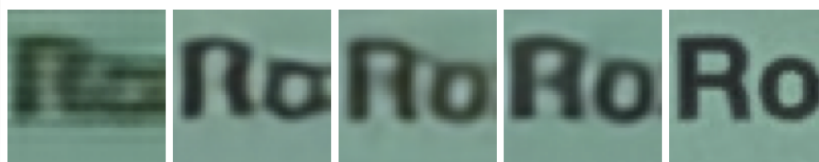
Bicubic

SRResNet

EDSR

ESRGAN

CDC



SRFlow

LP-KPN

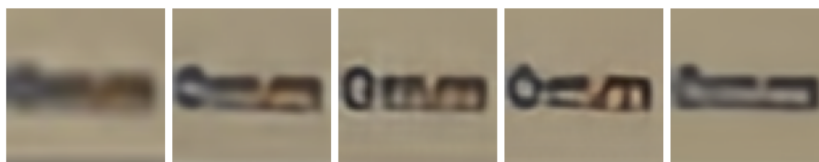
RCAN

Ours

HR



Nikon_024 (x4)



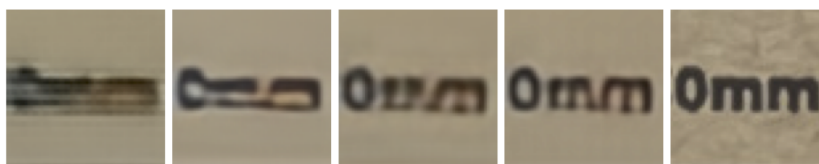
Bicubic

SRResNet

EDSR

ESRGAN

CDC



SRFlow

LP-KPN

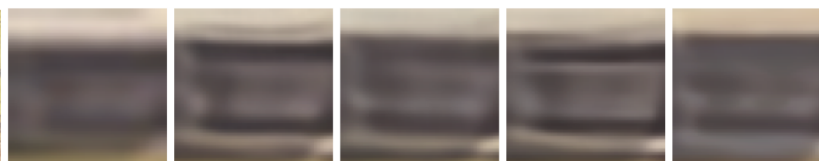
RCAN

Ours

HR



Canon_008 (x4)



Bicubic

SRResNet

EDSR

ESRGAN

CDC



SRFlow

LP-KPN

RCAN

Ours

HR

Figure 11. More visual comparison results.

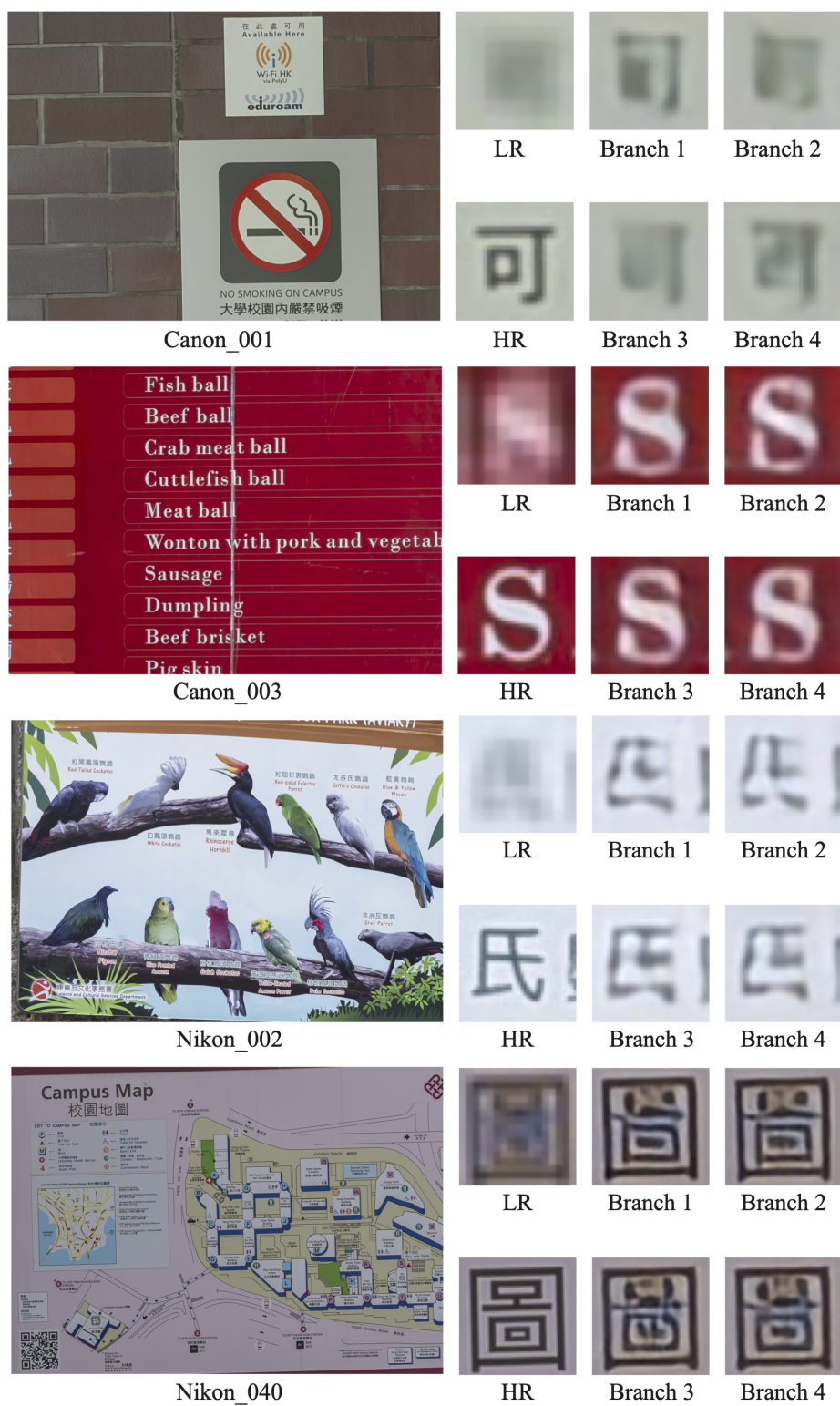


Figure 12. More visual divergence results.